Overview

Prediction of two-dimensional materials by the global optimization approach

Teng Gu,[1,2] Wei Luo[1,2] and Hongjun Xiang[1,2]*

Crystal structure prediction is one of the most fundamental challenges in the physics and chemistry sciences. In recent years, this problem has gained much practical success by the global optimization approach. Here, we survey some recent progress in finding the global minimum of two-dimensional (2D) materials, and introduce some details of these global optimization approach. Then, we will give some typical examples to demonstrate their advantages for 2D crystal structure prediction. Finally, the future directions and challenges are briefly discussed.

How to cite this article:
WIREs Comput Mol Sci 2017, 7:e1295. doi: 10.1002/wcms.1295

INTRODUCTION

Graphene, a single layer of carbon atoms with a honeycomb configuration, has attracted much interest due to its massless Dirac Fermion, quantum Hall effect, and ultrafast carrier transport ability.[1–8] Because of its extraordinary properties, graphene has many potential applications, such as transparent electrodes, optical devices, and storage.[9–11] Motivated by the great success of graphene, more and more 2D materials were studied in recent years.[12] Monolayer MoS_2, which has a direct band gap, can be used as field-effect transistors (FETs) and other optoelectronic devices. It was showed that it has lower power consumption and higher luminescence quantum efficiency than classical transistors.[13–15] Phosphorene has become another rising star after graphene. It has a quasi-direct band gap and show good mobility, good flexibility, and interesting anisotropic properties.[16–19] Other 2D materials such as boron nitride (BN), SiC sheet, and silicene[20–23] also exhibit their own unique properties.[24,25]

Up to now, only a few 2D materials have been synthesized.[26–30] As we know, the experimental cost is huge in many cases. Although some 2D structures were proposed, they may be not the global minimum structures and may be difficult to be synthesized. Hence, finding the global minimum structure is the key for discovering novel 2D materials.

Crystal structure prediction is one of the most challenging tasks in material sciences. Thanks to the significant progress in computational power, various advanced methods for crystal structure prediction have been developed and applied in the past decades. These methods include simulated annealing,[31–33] genetic algorithm (GA),[34–41] basin hopping,[42,43] metadynamics,[44,45] random sampling,[46–48] particle swarm optimization (PSO),[49–51] and *ab initio* random structure search.[52] Some methods have been used to 2D structure prediction. In 2011, Luo et al. first proposed a method based on the PSO algorithm to predict the single-atomic layer crystal structure.[53] After that, based on PSO algorithm, Luo et al. proposed a new method to predict 2D crystal structure with finite thickness.[54] The GA was also adopted to predict 2D structures.[55,56] The data mining method was extended to explore the 2D materials,[57] but it relies on the existence of an extensive database of International Crystallographic Structural Database (ICSD) and is incapable of generating

*Correspondence to: hxiang@fudan.edu.cn

[1]Key Laboratory of Computational Physical Sciences (Ministry of Education), State Key Laboratory of Surface Physics, and Department of Physics, Fudan University, Shanghai, P. R. China

[2]Collaborative Innovation Center of Advanced Microstructures, Nanjing, P. R. China

Conflict of interest: The authors have declared no conflicts of interest for this article.

new crystal structure types in the absence of information on similar compounds.

In this review, we focus on these global optimization methods (mostly evolutionary algorithms) that have been applied to predict the 2D materials. First, the details of algorithms will be presented. Then, some typical applications will be introduced. Finally, we briefly discuss the potential challenges and future directions for the 2D structure prediction.

EVOLUTIONARY ALGORITHMS FOR 2D CRYSTAL STRUCTURE PREDICTION

Up to now, most studies on predicting 2D materials adopted the evolutionary algorithms (EAs), such as GA, PSO, and differential evolution (DE) algorithm. Hereafter, we will present the details of these algorithms.

Potential Energy Surface

The crystal structure of 2D materials is periodic in the lateral plane and have a finite extent in the third dimension. It is useful to describe the dimensionality of the crystal structure with three lattice parameters (the lengths of the two lateral lattice vectors and the angle between them) and 3N-3 atomic coordinates, where N is the total number of atoms in the unit cell. The potential energy surface (PES) is used to characterize the energy as a function of the 3N dimensional parameters. The global optimization problem is an nondeterministic polynomial-time hard (NP-hard) problem, because finding the global minimum with certainty presumably involves visiting every local minimum and the number of minima in the PES of a large system increases exponentially with the number of atoms.[52,58] With such high-dimensional problems, simple exhaustive search strategies are clearly unfeasible.

The global optimization problem can be greatly simplified if considered some general properties of PES.[59,60] First, many high-energy structures can be neglected, e.g., when some atoms are very close to each other. Second, local optimization can simplify the problems as well. A basin of attraction of a PES is defined as the set of points for which downhill relaxation leads to the same energy minimum. Figure 1 illustrates how local optimization transforms each basin of attractions of PES into a flat platform, which dramatically simplify the search space.

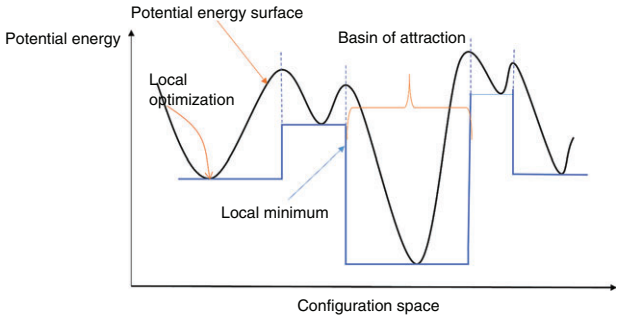

FIGURE 1 | Illustration of the potential energy surface. The use of local optimization can reduce the potential energy surface to simple steps.

Details of the Evolutionary Algorithms

Overview

The EA, as the kernel of many global optimization approaches, is based on simple concepts arising from natural phenomenon. Each crystal structure is analogous to a single organism. The fitnesses of organisms are based on their objective function values, and they are allowed to reproduce depending on those fitnesses. There are several EAs to predict 2D crystal structures, which have been proved that they are well suited to the structure prediction. One is GA, which is stimulated by the biological evolution in nature.[37,39,61–66] Second, the PSO algorithm, which is inspired by the choreography of a bird flock and can be seen as a distributed behavior algorithm.[49–51,54,67–71] Third, the DE, which is an EA that optimizes an objection function by maintaining a population of candidates and creating new ones through mutation and crossover operations based on the differentials of the existing ones.[72–74]

The procedure of EA includes five steps as depicted in Figure 2: (1) generation of initial structures; (2) local structural optimization; (3) evaluation of fitness; (4) generation of new structures; (5) check convergence. Candidate structures are organized into groups called generations. The procedure proceeds by creating successive generations. All of the EA that we will be discussing in the following sections are based on these five steps to explain how the procedures operate.

Generation of Initial Structures

In general, two types of variables are necessary to define a crystal structure: lattice parameters and atomic coordinates. Each 2D structure has three lattice parameters (lengths a, b, and angle γ) and 3N-3 atomic coordinates. Besides, quasi-2D (Q2D) and 2D

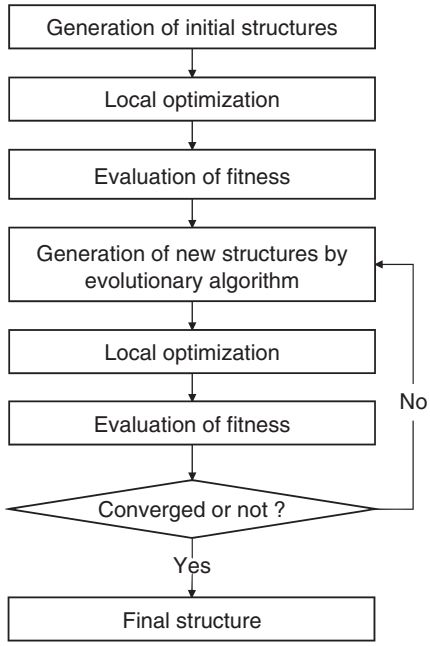

FIGURE 2 | The main flow chart of evolutionary algorithm for the structure prediction.

crystal structure can be characterized by 80 layer space groups and 17 planar space groups, respectively.[75] To ensure unbiased sampling of the energy landscape, the lattice parameters and atomic positions are randomly generated but confined within a chosen group symmetry. Once a particular space group is selected, the appropriate symmetry operations can be easily obtained. If there is an atom at point $A(x_1,x_2,x_3)$, the coordinates of the other atoms are generated by the crystallographic symmetry operations through matrix-column pairs (W, w), where the point operation W is a 3×3 matrix and the translation operation w is one column. The new atomic coordinate is obtained by the following matrix multiplication.[49,51]

$$\tilde{x_1} = W_{11}x_1 + W_{12}x_2 + W_{13}x_3 + \omega_1$$
$$\tilde{x_1} = W_{21}x_1 + W_{22}x_2 + W_{23}x_3 + \omega_2$$
$$\tilde{x_1} = W_{31}x_1 + W_{32}x_2 + W_{33}x_3 + \omega_3$$

After the candidate structure is produced, it is useful to test against some hard constraints: (1) Atom-dependent minimal interatomic distances; (2) The minimum and maximum values of the angle γ; (3) The minimum and the maximum lattice length; (4) The layer thickness of the 2D structure. If the candidate structure violates at least one of these constraints, it should be removed. The application of hard constraints can reduce the search space significantly. For the detail of the hard constraints, the distance between two atoms should not be lower than a threshold. Bahmann et al. set the threshold as 80% of the sum of the covalent radii of the two corresponding atoms to avoid too short bond lengths.[68] The angle γ is free to vary between 45° and 135°.[59] This is sufficient to represent all forms of 2D crystal structures. The minimum lattice length is chosen to be the sum of the typical bond length and the diameter of the largest atom in the system.[62,64,76] Bahmann et al. set the maximum lattice vector length to the sum of the covalent diameters of all atoms in the cell.[62] The layer thickness is unique to the 2D structure. This is an empirical parameter since different materials might have different thickness.

Local Structural Optimization

Local structural optimization is one of the most important features of all high-efficiency global optimization programs. The local optimization such as line minimization, steepest descents, or conjugate gradient algorithm can drive the total energy to the local minimum,[37,77] which might increases the cost of each individual, but effectively reduces the noise of the landscape (see the section *Potential Energy Surface*), and facilitates the comparison between different structures.[49,64] Almost all local structural optimizations were carried out with the first principles codes, such as Quantum ESPRESSO package[78] and VASP (Vienna *ab initio* simulation package).[79]

The *ab initio* package not only provides locally optimized structures for further usage but also provides many properties of the locally optimized structures. Properties such as the total energies or band gap can be used as fitness throughout the simulation.[72,80]

Evaluation of Fitness

There are two kinds of properties which we need to evaluate for each generation. One is the fitness of an organism, which is the property on which evolutionary pressure acts. It depends on the value of the objective function, and better solutions have higher fitness. Wang et al.[49] and Glass et al.[64] used the negative of the *ab initio* total energy of the locally optimized structure as fitness value. Differently, Tipton et al.[81] normalized the fitness in the context of its generation. In particular, an organism with an objective function of value k is assigned a fitness f given by

$$f = \frac{k-a}{b-a}$$

where a and b are the objective function values of the worst and best structures in the current generation, respectively. In this case, the organism with the lowest energy in the generation is assigned a fitness of 1, and the organism with the highest energy has a fitness of 0.

Multiobjective optimization approaches based on EA were also proposed.[72,82] In these approaches, the objective of structure is not only the total energy but also other properties of the material. Revard et al. employ the layer thicknesses of 2D materials as the second objective function. According to Zhang et al., the users can define their own second objective function. For example, the band gap and/or bulk modulus can be defined as the other objective function to find desirable functional materials.[46]

Another is the similarity test. When the EA progresses, many newly generated structures are very similar or even identical to the old structures in the population. If a pair of structures mate more than once, they are likely to create similar offspring. As the time goes by, all the organisms are likely to become more similar. The direct use of these similar structures to generate next generation will significantly slow down the convergence to the global minimization solution,[49,83] and low diversity in the population makes it difficult for the algorithm to escape local minima and to explore neighboring regions of the PES.[59] For these reasons, it is desirable to maintain the diversity of the population by identifying and removing equivalent structures.

Tipton et al. directly compare atomic positions to identify duplicate structures in the population.[81,82] During the search, two separate lists of previously observed structures are maintained. The first list, holds the relaxed, developed structures which are members of the current generation. If a new relaxed offspring structure matches one of the structures in this list, it is discarded to avoid having duplicate structures in the generation. Similarly, the next list holds all structures the algorithm has seen, both relaxed and unrelaxed. If a new unrelaxed offspring structure matches one of the structures in the list, it is discarded. This approach not only minimizes the number of redundant calculations performed but also prevents the population from stagnating.

Wang et al. established a bond matrix to determine whether two structures are identical.[49] The components of the matrix are the distances and number of the first and second nearest neighbors for different bond types. In a slightly different way, Bahmann et al. identify duplicate structures by choosing a central atom in each organism and comparing the bond lengths between the central atom and the other atoms in a supercell.[62] Zhang et al. defined a bipartite graph that describes essential characteristics of two structures.[72] This is the most rigorous methods, but the cost of computational complexity increases. The similarity of the two structures is the total Euclidean distance between two structures. The smallest total distance between two structures can be solved by Kuhn–Munkres algorithm.[84] If the total distance is below a certain threshold, one of the structures will be eliminated.

Generation of New Structures

The core of the EAs lies in the way how the offspring structures are generated from the parent. This is an important part of the algorithm because it is the only way that the algorithm guides the population toward the global minimum.

Selection

Before generating a new organism, the algorithm selects one or more structures to serve as parents based on their fitness. There are several commonly used selection strategies. In the truncated selection, some fractions of the best organisms in the generation are allowed to act as parents with equal probability, while the rest are prevented from mating.[85] In the tournament selection, all of the organisms in the parent generation are randomly divided into small groups, and then the best member of each group is selected to act as parents. Finally, in roulette wheel selection, the probability that an organism is selected to act as a parent is directly proportional to its fitness.

Glass et al. use truncated selection to remove some fraction of the parent generation, and then choose linear or quadratic probability distribution over their fitness to get offspring.[59,64] Tipton et al. developed a similar but more general strategy to select parents.[81] Bahmann and Zhang et al. simply chose parent structures randomly from the population.[62,72] The preference of the random choice is due to the fact that it enhances diversity of the children.

After selecting the parents, one can adopt GA, PSO, or DE algorithm to generate new offspring. In the following, we will describe these EAs in detail.

Evolutionary Algorithms

Genetic Algorithm

Mating. The energy of the crystal materials is a short-ranged property. Therefore, mating operation is the most commonly used approach. This approach

extracts a coherent segment or real-space slice of a parent structure, and then stacks them on top of another segment or slice extracted from another parent using the same extracting process. In this way, the energy minimization problem has high heritability.

After two parent organisms have been selected, the next step is choosing the planes along which to slice them. In the work of Bahmann et al.[62] one lattice vector b is picked randomly, all atoms in one of the parent organisms are shifted along the lattice vectors. When the shift was performed, a fractional coordinate s along b were randomly chosen. All atoms in one of the parent organisms with a fractional coordinate greater than s along b and all atoms in the second parent with fractional coordinate less than or equal to s are copied to the new child. With a slightly different method, Tipton et al. selects a slice inside of the parents.[81] Randomly selected fractional coordinate acts as the center of the slice, then the slice thickness is randomly chosen from a Gaussian distribution, and the two slice planes are placed accordingly. The principle of mating operator is illustrated in Figure 3.

An offspring organism produced via mating as described so far may have a different number of atoms or a different composition than its parents. Bahmann et al. constrain the total number of atoms of each type is equal to parents.[62] If there are too many atoms of a type, atoms of this type are removed randomly. If there are too few, first, an interval is picked in inverse proportionally to the atom density, then one atom of this type is added randomly in this interval. The procedure is repeated until the number of atoms is correct.

Mutation. Mutation is considered as a vital part of EAs, because of its ability to explore the area in the vicinity of the parent, and the closeness of low-lying minima location in the energy landscape.[86] The common mutation is selecting one individual and use to produce offspring by randomly perturbing the atomic positions or lattice vectors. The mutation of lattice vectors is by applying a randomly generated symmetric strain matrix:

$$[I+\varepsilon_{ij}] = \begin{bmatrix} 1+\varepsilon_{11} & \frac{\varepsilon_{12}}{2} & 0 \\ \frac{\varepsilon_{12}}{2} & 1+\varepsilon_{22} & 0 \\ 0 & 0 & 1 \end{bmatrix}$$

where I is the unit matrix and $_{ij}$ are zero-mean Gaussian random variables.[62,64,81] Note that there are only four free strain variables for a 2D system. According to Glass et al., the new offspring will be scaled to a specified volume that the parent has,[64] while Bahmann et al. did not do volume rescaling in order to avoid unnecessary narrowing of the search.[62]

Mutations of the atomic positions are achieved in a similar way. Each of the three spatial atomic coordinates is perturbed by a zero-mean Gaussian distribution.[62,64,81] Owing to diversification within mating and local optimization, mutations of the atomic positions are not important and can be omitted.[64]

Another mutation operation proposed by Tipton and Glass[64,81] is exchanging different types of two atoms, which facilitate finding the correct atomic ordering but apply only to systems with different types of atoms. It is usually helpful to use a permutation variation when studying these systems in order to find the minimum among several competing low-energy configurations. Tipton et al. considered the random addition or removal of atoms.[81] It has the capacity to look for a broader PES.

Particle Swarm Optimization

In this scheme, unlike the GA, each individual structure is regarded as a particle (or a bird). Each particle has a position and a velocity, where the velocity determines how position evolves.[49] The positions of offspring particles are updated according to the evolution equation as follows:

$$x^{t+1} = x^t + v^{t+1}$$

$$v^{t+1} = wv^t + c_1 r_1 (pbest^t - x^t) + c_2 r_2 (gbest^t - x^t)$$

where x^t is the previous location before optimization, v^t is the previous velocity, $pbest^t$ is the current location after structural optimization, and $gbest^t$ is the

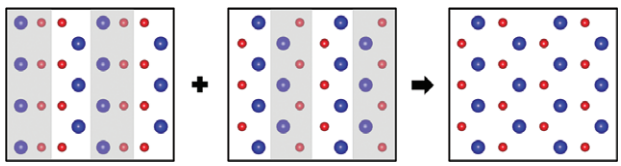

FIGURE 3 | Illustration of how the mating operator works: parent structures are sliced and combined to form an offspring structure. For clarity, 1 × 2 supercells are shown. (Adopted from 'Grand-canonical evolutionary algorithm for the prediction of two-dimensional materials')[82]

population global location with the best fitness value for the entire population. In this expression, the velocity plays an important role in determining the speed and direction of particle movement. The inertia weight w, c_1 and c_2 control the momentum of the particle. Generally, w is in the range of 0.4–0.9. Higher value of w such as 0.9 facilitates global search, and lower value facilitates rapid local search. According to the Wang et al., w is dynamically varied and decreases linearly from 0.9 to 0.4 during the iteration. r_1 and r_2 are random numbers which range from 0 to 1. The evolution schematic diagram of velocity and position are showed in Figure 4.

Lyakhov and Oganov employ fingerprint distances[39,87] to distinguish the difference between two particles in cell parameters and atomic coordinates. Instead of applying at each step, all moves with same weights. They combined GA with the PSO to form two variation operators.[39] The particle is either mutated (to imitate a random move), or participates in heredity with its best known position or in heredity with the best known population position (to imitate PSO moves in the direction of these positions). They apply them one by one with a certain probability.

DE Algorithm

The goal of the DE is to combine the difference of two parents with the best solution in the parent population as the structural characteristics in a single organism.[72,88] The following evolution operator is applied to generate offspring:

$$p_i' = \gamma p_{best} + (1-\gamma)p_i + F(p_{r1} - p_{r2})$$

where p_i is a vector which represents a solution of the parent population, p_{best} is the population global location with the best fitness value for the entire parent population. p_{r1} and p_{r2} are randomly selected from the parent population. γ and F are scale factors in the range of [0, 1].

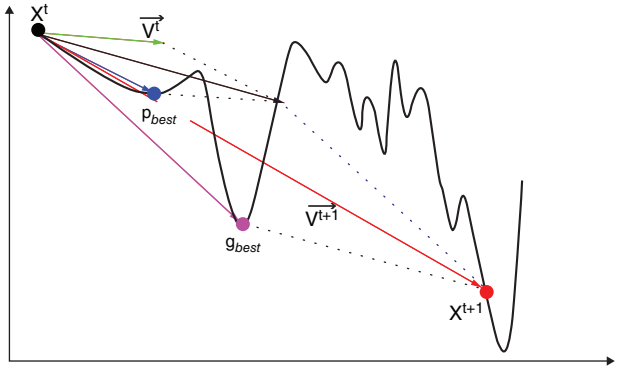

FIGURE 4 | Illustration of how the velocity and position updates in particle swarm optimization. The black solid line represents a typical potential energy surface. Arrows represent either the positions or the velocity of a particle. (Adopted from 'Crystal structure prediction via particle swarm optimization')[49]

Besides the above EAs, DE also generates some new offspring randomly in order to increase the diversity of the population. For each newly generated offspring, one should check whether the hard structural constrains are satisfied. If not, this offspring is discarded.

Summary of Algorithms

It has been observed that EAs are well suited to the structure prediction. They can efficiently find the global minimum of multidimensional PES. Besides, EAs require little information and few assumptions about the system, which is advantageous when we do not have any prior knowledge of systems. The EAs incorporate 'learning from history.' To be more specific, for PSO and DE, their offspring just depends on the best fitness value for the entire parent population and one or two parents, which is easy to be programmed. For GA, there are more complicated variation operators. However, EAs have a potential shortcoming. One can never prove that the 'global minimum structure' found by EAs is the true global minimum structure. For example, initially, the BSi_3 structure was proposed to be an alternate arrangement of zigzag single-Si atom chains and silicon – boron chains.[89] Later, a lower energy structure of BSi_3 which contains a planar aromatic D_{6h} c—Si_6, and a strong π – p conjugation between c-Si_6 and B atoms was discovered.[90]

There are some production codes available to users. GA is the kernel of the Universal Structure Predictor: Evolutionary Xtallography (USPEX) code,[39,64] Evolutionary Algorithm for Crystal Structure Prediction (EVO) code[62] and Grand-canonical Genetic Algorithm for Structure and Phase Prediction (GASP) code.[81] PSO algorithm is adopted by Crystal structure Analysis by Particle Swarm Optimization (CALYPSO) code.[49,50] DE is implemented in the Inverse design of Materials by Multi-Objective Differential Evolution (IM^2ODE) code.[72] These codes can be adopted to predict 2D materials. However, they are not efficient for big system. The efficiency might be improved if an accurate potential can be developed.

Check Convergence

In principle, the global minimum of the energy landscape will be found by the EAs in the limit of infinite number of generations,[88] but this is practically impossible. There are some techniques to analyze the success rate of the evolutionary algorithms and stop the search. One common technique to analyze the

success rate of an EA was given by Hartke.[91] The data are generated on the same system, then the lowest energy, the highest energy, and the average energy in each generation are recorded and plotted to describe the success of the EA. In this way, the lowest and highest energies encountered are outliers, and in practice they depend strongly on the number of independent structures. Therefore, Tipton et al. employs 10th and 90th percentiles energies of the best structures to replace the lowest energy and the highest energy. The 10th and 90th percentiles offer a better characterization of the distribution of results and are less susceptible to outliers and the number of independent structure searches performed to characterize the efficiency of the algorithm.[81]

A common approach to stop the search is if a user-specified number of generations have passed without improvement of the best organism.[49,62,64,72,81] Bahmann et al. have determined convergence when the diversity of the offspring is too low or when all the organisms have very similar energies.[62] The default halting criterion in CALYPSO is when the simulation could not find other stable structures[50] with 10 further generations.

APPLICATIONS

EAs have been used to predict 2D materials. In this section, a comprehensive review of previous applications will be presented. We group these applications into two categories: single-atomic layer systems and multilayer systems.

Single-Atomic Layer Systems

We list the single atomic layer materials which were predicted by EAs in Table 1. The information listed in this table includes the chemical formula, the maximum number of atoms in the search, the EA code used, and the first author.

Single Element Materials

Single-Layer Boron

It was proposed that boron might possess freestanding flat monolayer structure. Wu and Yu et al. found several possible boron sheets composed of triangular and hexagonal motifs by using the global optimization method. Soon afterwards, Lu et al. found that there exist two types of stable monolayer boron sheets with

TABLE 1 | Predicted Single Atomic Layer Systems with Evolutionary Algorithms

Chemical Formula	Number of atoms (m)	EA code	References
B_n	4,6,8,10,12,14	CALYPSO	Wu et al.[92]
B_n	$2 \le n \le 40$	—	Lu et al.[93]
B_n	$n \le 16$	CALYPSO	Yu et al.[30]
C_n	6,8,10,12,14,16,18,20,22,24	USPEX	Wang et al.[94]
CO, C_2O, C_3O, C_4O	$m \le 16$	—	Xiang et al.[95]
C_3N, $C_{12}N$	—	CALYPSO	Xiang et al.[96]
SiC_n n = 3/2, 3, 4	$m \le 10$	CALYPSO	Li et al.[97]
Cu_2Si	3, 6, 9, 12, 15, 18	CALYPSO	Yang et al.[98]
SiC_2	—	CALYPSO	Zhou et al.[99]
Al_nC n = 1/3, 1, 2, 3	$m \le 16$	CALYPSO	Dai et al.[100]
SiC_3	$m \le 16$	CALYPSO	Ding et al.[101]
$(Al_2C)_n$	6, 12	CALYPSO	Li et al.[102]
BSi_4, BSi_3, BSi_2, BSi, B_2Si, B_3Si, B_4Si, B_5Si, B_6Si, B_7Si	$m \le 42$	CALYPSO	Dai et al.[89]
$(BSi_3)_n$	$n \le 3$	CALYPSO	Tan et al.[90]
$B_{x/2}N_{x/2}C_{1-x}$ (0 < x < 1) x = 2/3, 1/2, 2/5, 1/3	12, 8, 20, 12	CALYPSO	Zhang et al.[103]
BC_5, BC_3, BC_2, BC, B_2C, B_3C, B_5C	$m \le 18$	CALYPSO	Luo et al.[53]
Be_2C	6, 12, 18	CALYPSO	Li et al.[104]
Be_5C_2	7, 14, 28	CALYPSO	Wang et al.[105]
FeB_2	3, 12, 27	CALYPSO	Zhang et al.[106]
FeB_6	7, 14, 28	CALYPSO	Zhang et al.[107]

CALYPSO, Crystal structure Analysis by Particle Swarm Optimization; IM^2ODE, Inverse design of Materials by Multi-Objective Differential Evolution; USPEX, Universal Structure Predictor: Evolutionary Xtallography.

similar stability.[93] The most stable boron sheets are composed of two kinds of elementary units with isolated-hexagon and twin-hexagon holes, respectively.

Single-Layer Carbon

Apart from the boron, single-layer carbon materials were theoretically examined. Wang et al. proposed a new low-energy 2D carbon allotrope, which was composed of 5-6-7 carbon rings.[94] This 2D carbon structure with *Pmg* plane group has the direction-dependent Dirac cones and proved to be robust against the external strain with tunable Fermi velocities.

Compound Materials

B–C Alloy

The 2D B–C alloy is the first 2D system whose stable structures were predicted by the EA. In 2011, Luo et al. systematically searched the 2D B–C compounds for a wide range of boron concentrations (BC_5, BC_3, BC_2, BC, B_2C, B_3C, and B_5C) via a modified version of CALYPSO.[53]

For carbon-rich compounds (BC_2, BC_3, and BC_5), the 2D sheets can be viewed as boron-doped graphene structures. Interestingly, there are isolated 1D zigzag boron chains in the most stable 2D structures of BC_5 (Figure 5(a)) and BC_2 (Figure 5(c)). In BC_5, the most stable 2D structure (Figure 5(a)) is energetically more favorable and has a much lower energy than previously announced structure[108,109] by 51 meV/atom. This might be due to the fact that this structure has more C—C π bonds. Different from BC_2 and BC_5, the 2D structure of BC_3 with uniformly distributed boron atom (Figure 5(b)) is more stable with 1D zigzag boron chains. For BC, the stable 2D

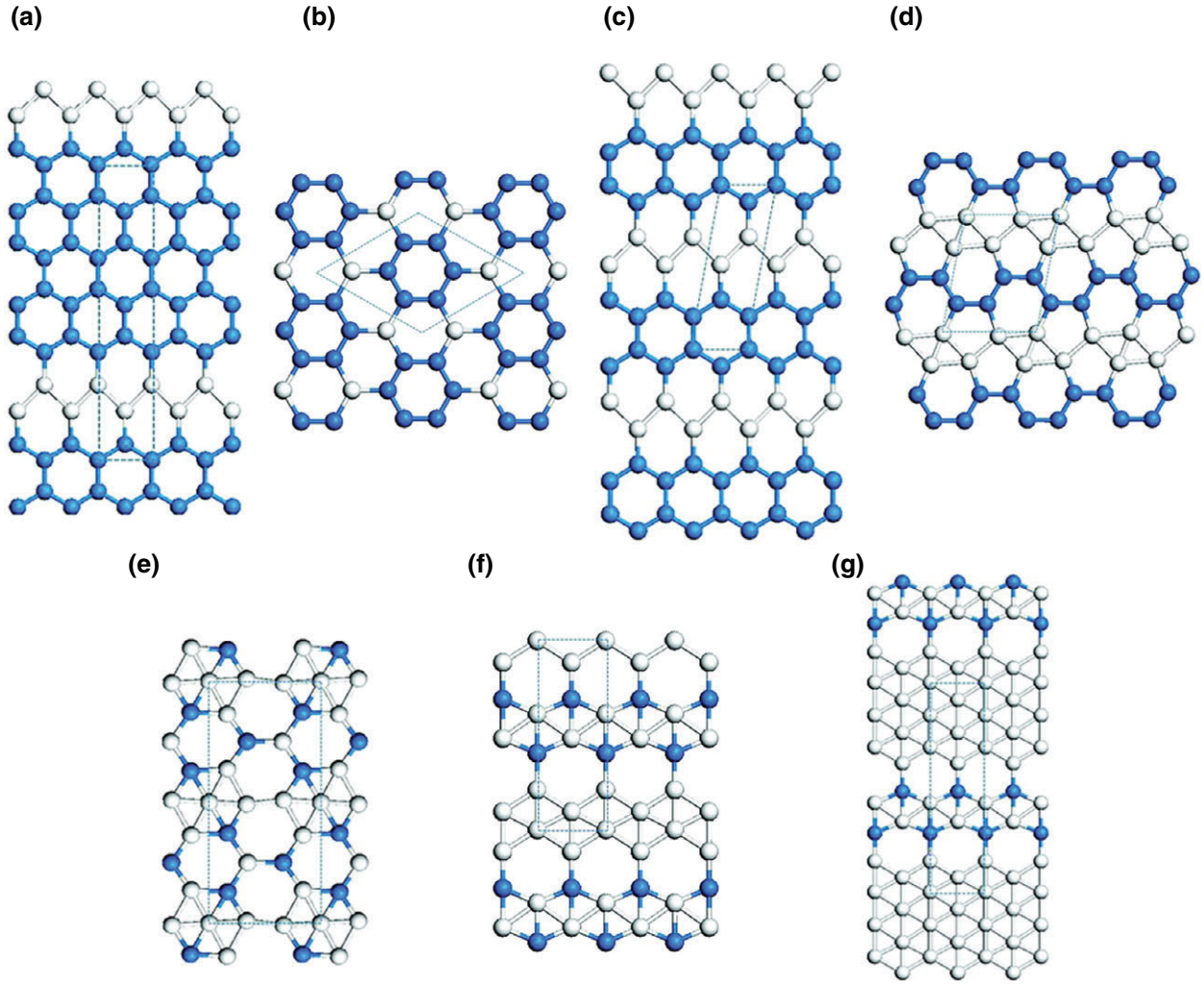

FIGURE 5 | The lowest energy of different BC Compounds 2D structures from the particle swarm optimization simulations (Color online). The C and B atoms are denoted by blue and gray atoms, respectively. (a) The lowest energy of BC_5, (b) the lowest energy of BC_3, (c) the lowest energy of BC_2, (d) the lowest energy of BC, (e) the lowest energy of B_2C, (f) the lowest energy of B_3C, and (g) the lowest energy of B_5C. (Adopted from 'Predicting Two-Dimensional Boron-Carbon Compounds by the Global Optimization Method')[53]

structure (Figure 5(d)) is strip like with alternative boron chains and armchair carbon chains. Every carbon atom is sp^2 hybridized, forming two C—C bonds and one B—C bond. Each boron atom consists of four neighbors with one B–C bond and three B–B bonds. Boron-rich compounds (B_2C, B_3C, and B_5C) has peculiar planar-tetracoordinate carbon (ptC) motifs and boron triangles, they do not resemble clearly the structural feature of α-sheet boron structures, in contrast to the carbon-rich case. For B_2C, the lowest energy 2D structure (Figure 5(e)) can be seen as the addition of boron atoms to the center of the B_4C_2 six-membered ring of the B_5C_3 graphene structure, which has a lower energy (49 meV/atom) than that of previous proposed structure by Wu et al.[110] The most stable 2D B_3C structure (Figure 5(f)) contains alternative zigzag boron chains and zigzag boron-carbon chains. The most stable 2D structure of B_5C (Figure 5(g)) is similar to B_3C except that the ribbon width of the triangular boron sheet is now four instead of two.

The electronic band structure calculations showed that all the 2D B–C compounds are metallic except for the most stable structure of BC_3. The metallicity stems from the delocalized $2p_z$ π electrons of carbon and boron atoms and the semiconducting behavior of the most stable structure of BC_3 is due to six-membered'benzene' rings isolated by boron atoms. The electron localization function analysis of the nature of bonding shows that the delocalized p states of 1D zigzag boron chain in the carbon-rich compounds and the three-center boron bonds in the boron-rich case play an important role in the structural stability.

C–N Alloy

Xiang et al. studied the collective behavior of nitrogen doping in graphene.[96] They found two stable, ordered structures of N-doped graphene: C_3N and $C_{12}N$, where the nearest-neighbor interaction between nitrogen dopants is highly repulsive as a result of the strong electrostatic repulsion between nitrogen atoms. Both structures are semiconducting. In particular, $C_{12}N$ has a direct band gap of 0.98 eV, which is a promising candidate for a new type of organic solar cell. The theoretical prediction on C_3N was partially confirmed experimentally by Zhao et al.[111]

C–Si Alloy

Both graphene and silicene are not suitable for FET applications due to their zero-band-gap nature. Some researchers tried to mix carbon and silicon atoms to tune the electronic properties. Zhou et al. predicted a novel planar SiC_2 siligraphene (g-SiC_2) with a direct band gap of 1.09 eV, in which Si and C atoms adopt sp^2 hybridization and C atoms form delocalized 4 C-domains that are periodically separated by Si atoms.[99] Ding et al. revealed three lowest energy structures for SiC_3 ones, all of which are Si-graphene hybrid honeycomb lattices with robust dynamical stabilities.[101] Depending on the ordered arrangement of Si atoms, the SiC_3 sheets could be direct-band-gap semiconductors or zero-band gap semimetals. Later, Li et al. systematically studied different stoichiometric compositions with Si:C ratio equal to 2:3, 1:3 and 1:4.[97] They predicted that many of the low-energy metastable and the lowest energy silicon–carbon structures are not graphene like. All of the studies on silicon–carbon structures showed that these 2D silicon–carbon compounds with different stoichiometric compositions may be exploited for future applications in nanoelectronic devices.

C–Be Alloy

Using the CALYPSO code, Li et al. found the global minimum structure of Be_2C monolayer, in which each carbon atom binds to six Be atoms in an almost planar fashion, forming a quasi-planar hexacoordinate carbon (phC) moiety.[104] The electronic properties show that Be_2C has a direct gap of about 1.52 eV, which is suitable for electronic and optoelectronic applications in the future. Later, Wang et al. found the lowest energy structure of 2D Be_5C_2 with the same method.[105] For Be_5C_2 monolayer, each carbon atom binds with five beryllium atoms in almost the same plane, forming a quasi-planar pentacoordinate carbon (ppC) moiety. It is semimetallic with a Dirac-like point and also has an unusual negative Poisson's ratio, which is expected to have wide applications in electronics and mechanics.

Fe–B Alloy

Zhang et al. studied the graphene-like 2D materials of Fe–B compounds.[106,107] For FeB_6 monolayers, three stable structures (α-FeB_6, β-FeB_6, and γ-FeB_6) are composed by the Fe©B_x (x = 6, 8) wheels with planar hypercoordinate Fe atoms locating at the center of six- or eight-membered boron rings. The α-FeB_6 monolayer is metallic, while the β-FeB_6 and γ-FeB_6 sheets are semiconductors with indirect band gaps and significant visible-light absorptions. For FeB_2 monolayers, they found that its global minimum structure is a Dirac material (in Figure 6) with a Fermi velocity in the same order of graphene. The electron transfer from Fe atoms to B networks not only effectively stabilizes the FeB_2 networks but also leads to the strong interaction between the Fe and B

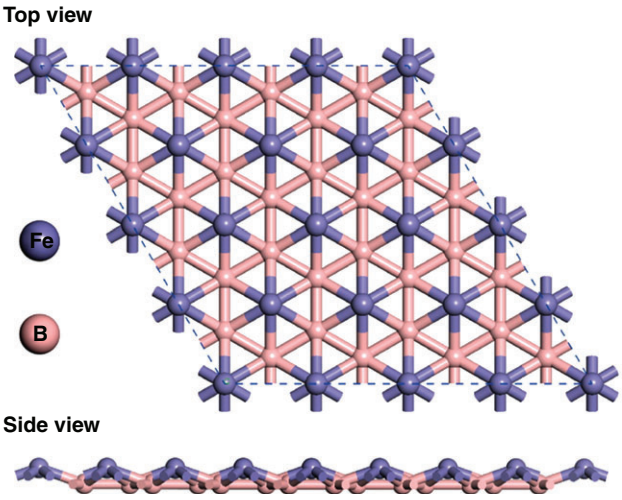

FIGURE 6 | The global minimum structure of FeB_2 monolayer from the particle swarm optimization simulations (Color online). The B atoms are arranged in a honeycomb lattice and Fe atoms are located above the center of hexagonal boron rings. (Adopted from 'Dirac State in the FeB_2 Monolayer with Graphene-Like Boron Sheet')[106]

atoms. These results provide a promising strategy to stabilize the 2D boron networks.

Other Monolayer Materials

Zhang et al. studied 2D $B_{x/2}N_{x/2}C_{1-x}$ (x = 2/3, 1/2, 2/5, and 1/3) compounds. Their results show that the band gaps of $B_{x/2}N_{x/2}C_{1-x}$ can be widely tuned within the optical range by changing the concentration of carbon, thus allowing the fast development of the band gap engineered materials in optoelectronics.[103] Li and Dai et al. studied 2D stoichiometric Al_xC (x = 1/3, 1, 2, and 3) monolayer sheets.[100,102] They found that the Al_2C monolayer is a semiconductor with an indirect minimum band gap and a slightly larger direct band gap, thus is suitable for photovoltaic applications. Dai et al. studied the 2D boron–silicon compounds.[89] For many structures, each Si atom is bonded with three B or Si atoms within the same plane, due to a preference of planar sp^2-Si motif. Later, Tan et al. found a lower energy structure of BSi_3, which contains a planar aromatic D_{6h} c-Si_6, and a strong π–p conjugation between c-Si_6 and B atoms.[90] Yang et al. predicted a novel monolayer Cu_2Si featuring planar hexacoordinate copper and planar hexacoordinate silicon.[98] This system is quite stable up to 900 K, and is predicted to be a nonmagnetic metal.

Multilayer Systems

Global optimization approaches were also adopted to predict Q2D materials with a finite thickness. Table 2 summarizes the theoretical prediction of layered materials.

Single Element Materials

Q2D Si

Multilayer silicon has attracted a lot of attentions since the discovery of silicene. For bilayer Si, it was believed that the most stable structure is the AA stacking configuration.[120,121] Instead, Luo et al. found a new bilayer structure which has a lower total energy than that of AA-Si by 41 meV/atom.[54] Afterwards, Guo et al. performed extensive searches for the most stable phases of

TABLE 2 | Predicted Multilayer Systems with Evolutionary Algorithms

Chemical Formula	Number of atoms (m)	EA code	References
B_n	6,8,10,12,14,16,18	USPEX	Zhou et al.[112]
B_n	18,20,22,24,26,28	USPEX	Zhou et al.[55]
B_n	6,8,10	USPEX	Zhao et al.[56]
Si_n	$2 \le n \le 36$	IM^{2}ODE	Guo et al.[113]
$(InP)_n$ $n \le 6$	—	GASP	Revard et al.[82]
$(SiS)_n$ $n \le 6$	—	IM^{2}ODE	Yang et al.[114]
BiOF	$m \le 24$	USPEX	Zhou et al.[115]
C_nH n = 4, 3, 2, 3/2, 1 CO	m = 16, 24, 32, 40, 48	CALYPSO	Gao et al.[116]
MoS_2	12	CALYPSO	Ma et al.[117]
Si_8H_2, Si_4H_2, Si_6H_2, Si_4H_4	$m \le 10$	CALYPSO	Luo et al.[54]
$(BiF)_n$ $n \le 8$	—	CALYPSO	Luo et al.[75]
P_8O_1, P_6O_1, P_4O_1, P_2O_1, P_4O_4, P_2O_3	$m \le 16$	CALYPSO	Luo et al.[118]
PdS_2	6, 12	CALYPSO	Wang et al.[119]

CALYPSO, Crystal structure Analysis by Particle Swarm Optimization; IM^{2}ODE, Inverse design of Materials by Multi-Objective Differential Evolution; USPEX, Universal Structure Predictor: Evolutionary Xtallography.

silicene from the monolayer to quadlayer.[113] The most stable bilayer silicene phase is the same as that obtained in previous work.[54,122] For trilayer silicene, the two most stable present a 2 × 1 periodicity with hexagonal and rectangular supercells, which have P121/m1 and P1 symmetries, respectively. The most stable structure of quadlayer silicene belongs to the P1m1 layer group with a 2 × 1 periodicity. The top and bottom two silicene layers in this phase present the perfect π-bonded chain structure.

The most stable phases of silicene from the monolayer to quadlayer are dynamically stable, as evidenced from the calculated phonon spectra. Their cohesive energies increase with increasing layer thickness. The electronic properties of the multilayer silicene phases show that the band gaps of these stable phases range from 0.5 to 1.5 eV. Their outstanding optoelectronic properties suggest that they are suitable for optical fiber communications and solar cells.

Q2D Boron

Q2D boron systems also have attracted many interests in recent years. Zhou et al. found an orthorhombic structure with the layer group P*mmn*, which is a Dirac material according to the first principle calculations.[112] Remarkably, Zhao et al. showed that conventional Bardeen–Cooper–Schrieffer (BCS) superconductivity in the stable 2D boron structures is ubiquitous with the critical temperature T_c above the liquid hydrogen temperature for certain configurations, which arise from multiple phonon modes.[56] Recently, Zhou et al. used the EA code to predict a 2D magnetic boron which composed of B_{20} clusters in a hexagonal arrangement.[55]

Compound Materials

P–O Alloy

Phosphorus oxide (P_xO_y) is a promising material with many novel properties.[123,124] Recently, Lu et al. experimentally demonstrated that phosphorus oxides not only have tunable band gaps, but also are much more stable compared with pristine phosphorene under ambient condition.[125] However, the detail of the structure of 2D phosphorus oxides was still unknown. To address this problem, Luo et al. systematically searched the lowest energy structures of 2D phosphorus oxides with different oxygen concentrations (P_8O_1, P_6O_1, P_4O_1, P_2O_1, P_4O_4, and P_2O_3).[118]

For low oxygen concentration, the most stable structures of P_8O_1 and P_6O_1 are of the dangling black phosphorus (BP) type, as shown in Figures 7 (a) and (b). For P_4O_1, its 2D structure also belongs to the dangling-BP type which was first proposed by Wang et al.[126] (Figure 7(c)). For P_2O_1, it contains not only the dangling P = O motifs but also the P-O-P motifs (Figure 7(d)), which is lower than that of previous proposed structure by Wang et al.[126]

For higher oxygen concentration, the lowest energy structures of P_4O_4 and P_2O_3 are shown in Figure 8. The lowest energy structure of P_4O_4 (Figure 8(a)) only contains P-O-P bridge motifs. Six phosphorus atoms and four oxygen atoms form a ring. Its band structure shows that P_4O_4 has a direct band gap and good optical absorption. Hence, they proposed that P_4O_4 may be appropriate for photoelectrochemical (PEC) water splitting application. For P_2O_3, there are two kinds of ferroelectric structures, P_2O_3-I and P_2O_3-II (Figure 8(b) and (c)). P_2O_3-I is the lowest energy structure with the thickness less than 1.4 Å. The phosphorus atoms form a honeycomb lattice and each phosphorus atom is surrounded by three oxygen atoms. All phosphorus atoms are located in the top plane and all oxygen atoms are located in the bottom plane. So, P_2O_3-I has a nonzero electric polarization perpendicular to the lateral plane and it is the thinnest ferroelectric materials (i.e., hyperferroelectric).[127] P_2O_3-II is the

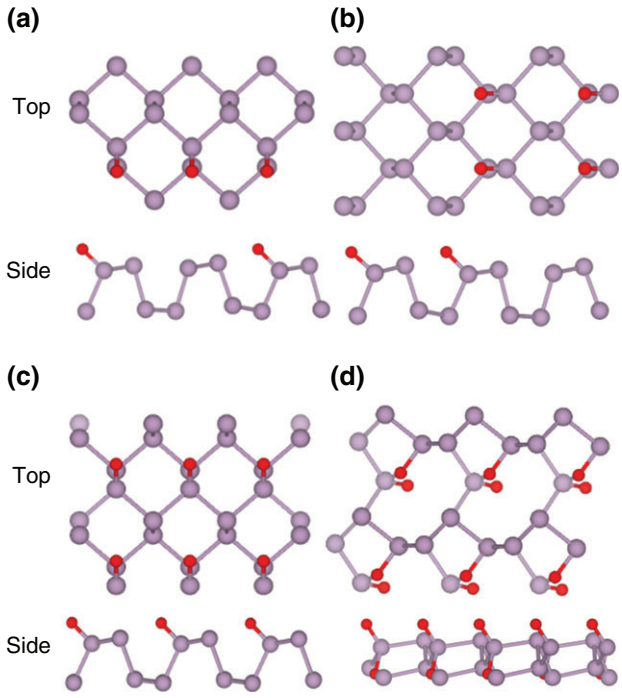

FIGURE 7 | The lowest energy of different PO Compounds 2D structures with thickness less than 3.2 Å. The P and O atoms are denoted by lavender and orange atoms, respectively. (a) The lowest energy of P_8O_1, (b) the lowest energy of P_6O_1, (c) the lowest energy of P_4O_1, and (d) the lowest energy of P_2O_1. (Adopted from 'Two Dimensional Phosphorus Oxides as Energy and Information Materials')[118]

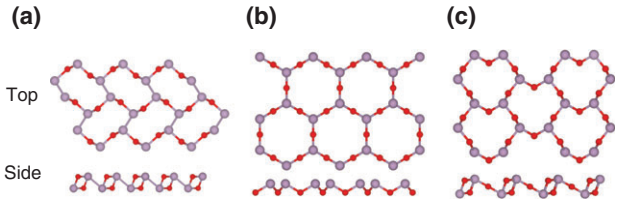

FIGURE 8 | Top and side views of P_4O_4 and P_2O_3. The P and O atoms are denoted by lavender and orange atoms, respectively. (a) The lowest energy of P_4O_4, (b) the lowest energy of P_2O_3 with thickness less than 1.4 Å, and (c) the lowest energy of P_2O_3 with thickness less than 3.2 Å. (Adopted from 'Two Dimensional Phosphorus Oxides as Energy and Information Materials')[118]

lowest energy structure of P_2O_3 with the thickness less than 3.2 Å. Its topology is similar with P_2O_3-I. Unlike P_2O_3-I, the phosphorus and oxygen atoms are no longer in the same plane. Owing to the collective oxygen displacements along the y axis, it has a nonzero polarization along the lateral plane.

Bi–F System

Quantum spin hall (QSH) effects,[128,129] also known as 2D topological insulators (TIs), are a new class of quantum materials. The most interesting character of TIs is the presence of robust helical edge states with spin locked to momentum as protected by time reversal symmetry. Currently, QSH was only observed at an extremely low temperature due to the tiny band gap. Hence, finding large band gap 2D Tis is important. In 2015, Luo et al. systematically studied the most stable Q2D structure of BiF through their developed methods.[54] They find that the global minimal Bi_4F_4 is a room temperature QSH insulator.[75] More calculations indicate that the Bi_4F_4 is thermally and dynamically stable.

Figure 9(a) shows the lowest energy structure (i.e., Bi_4F_4) among all structures with the thickness less than 6.0 Å. The Bi_4F_4 takes a distorted square lattice with two slightly different lateral lattice constants. It can be seen as a three layers structure: a bismuth layer with the distorted buckled square lattice is sandwiched between two BiF_2 layers. The local density approximation (LDA) band structure of Bi_4F_4 is shown in the left panel of Figure 9(b): Dirac cone at the Fermi level close to the Y point, after including the SOC effect, the band gap opens at the Dirac point. The electronic structure of Bi_4F_4 can be described rather well by a new TB model on a buckled square lattice, which shows that the band inversion is due to the chemical hybridization between the p_x and p_y orbitals.

Si–H Alloy

Although the majority of solar cells fabricated to date have been based on three-dimensional (3D) silicon, it is well-known that 3D bulk Si is not an ideal material for optoelectronic applications due to its indirect band gap.[130] Using the developed method,[54] Luo et al. studied several hydrogenate Si-layered structures.[54] For Si_8H_2, Si_8H_2-P*m11* is the lowest energy structure among all structures with thickness less than 6.0 Å. The hydrogen atoms only absorb at the bottom side. It has a lower energy by 73 meV/atom than the previously proposed structure.[120] Except for the two threefold coordinated Si atoms on the top surface, all the other Si atoms are fourfold coordinated. The two threefold coordinated Si atoms form a one-dimensional zigzag chain. For Si_6H_2, Si_6H_2-P*mm2* is the lowest energy among all Q2D structures with a thickness of less than 6.1 Å. There are four different kinds of Si atoms. Each Si atom is fourfold coordinated, indicating that this structure is highly stable. For Si_4H_2, Si_4H_2-P*3m1* is the lowest energy structure. Each Si atom is fourfold coordinated, forming good sp^3 hybridization. For Si_4H_4, Si_4H_4-P*man* is the most stable structure. It is based on the BP structure and has a lower energy than that based on the silicene structure by about 4 meV/atom. The band gap tends to increase with the concentration of hydrogen because the Si atoms can form better sp^3 hybridization when there are more H atoms. The direct band gap of Si_8H_2-P*m11* and Si_6H_2-P*mm2* are 0.75 eV and 1.59 eV, respectively, which is suitable for solar-energy absorber applications.

C–O Alloy

Xiang et al. investigated oxidized graphene on the basis of the GA.[95] For fully oxidized graphene C_1O, two low-energy semiconducting phases have been found. In one phase, parallel epoxy pair chains are running along the zigzag direction, in which has an indirect band gap of about 2.14 eV and an extremely low CBM that is below the Fermi level of graphene. Experimental evidence of this C_1O structure was reported later by Mattson et al.[131] The other C_1O phase has three mixed epoxy groups: normal epoxy, unzipped epoxy, and epoxy pair. For partially oxidized graphene, they predicted a phase separation between bare graphene and fully oxidized graphene. This phase separation was also confirmed experimentally later.

Other Materials

Wang et al. found PdS_2 monolayer presents rather unique structural properties: each Pd atom binds to four S atoms in the same plane, and two neighboring S atoms can form a covalent S–S bond, which is distinguished from other 2D transition metal disulfides.[119] The PdS_2 monolayer is semiconducting with

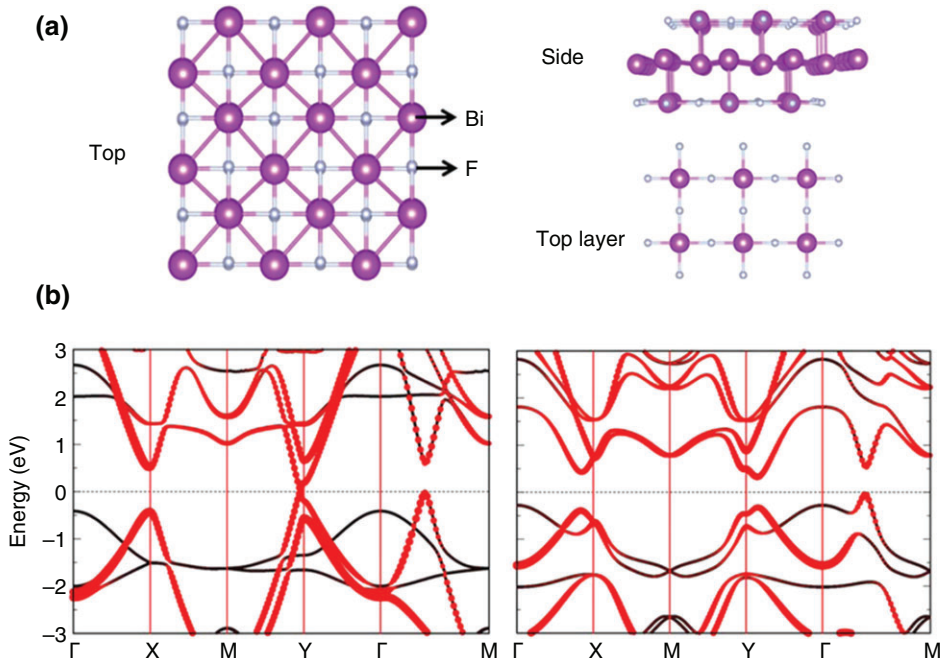

FIGURE 9 | Geometrical and electronic structures of Bi_4F_4 (Color online). (a) Top and side views of Bi_4F_4 and (b) local density approximation band structures of Bi_4F_4 without (left) and with (right) SOC. (Adopted from 'Room Temperature Quantum Spin Hall Insulators with a Buckled Square Lattice')[75]

an indirect band gap of 1.60 eV, and has a rather large hole and electron mobilities. Yang et al. found two kinds of 2D SiS materials that are energetically and thermally stable.[114] These 2D SiS materials have direct band gaps that are suitable for solar cell. In addition, their mobility is also rather high, maybe good materials for FET. Gao et al. studied the systems of hydrogenated graphene. They found that the band gap can be tuned by the hydrogen content easily.[116] Zhou et al. investigated the evolution of BiOF structures under pressure.[115] They found that BiOF can maintain its layered structure up to 300 GPa. Ma et al. discovered a new phase of MoS_2.[117] The new MoS_2 phase possesses a relatively large gap of 0.42 eV and there is a topological phase transition that can be simply controlled by a small tensile strain.

SUMMARY AND OUTLOOK

In this review, we have introduced the recent developments in predicting 2D materials by global optimization techniques. The energy minimization problem has been effectively addressed by EAs as described in section *Evolutionary Algorithms for 2D Crystal Structure Prediction*. Global optimization methods can find the lowest energy structure effectively in the case of several to dozens of atoms in the unit cell. Many successful applications are presented in the section *Applications*. We expect that more novel 2D materials can be predicted and synthesized by experiment in the near future.

Despite of the great success in 2D structure prediction, there remain a number of challenges need to be addressed. First, although considerable progress has been made in the use of phenotype operators, more intelligent and general methods (such as multiple neural network algorithm and machine learning) shall be developed to improve the efficiency. Second, the local optimization with the *ab initio* code is heavy. Hence, developing new local optimization code is important. Since the peak arithmetic and memory bandwidth of graphic processing unit (GPU) is much higher than that of the central processing unit (CPU),[132] GPU computing is more powerful for structural optimization at a large size. It is desirable to develop GPU-based code to perform local optimization. In addition, increasing the efficiency of the search through solution representation and variation operators is also a promising way of improvement. Another promising but challenging direction would be predicting 2D material on a given substrate, as we know, free standing 2D materials are not very stable, but many 2D materials can be stable on appropriate substrate. Hence, predicting 2D materials on a given

substrate may be a good direction and may lead to many novel physical or chemical properties because of the interaction between the 2D materials and substrates.

ACKNOWLEDGMENTS

Work was supported by NSFC (11374056), the Special Funds for Major State Basic Research (2015CB921700), Program for Professor of Special Appointment (Eastern Scholar), Qing Nian Ba Jian Program, and Fok Ying Tung Education Foundation.

REFERENCES

1. Novoselov KS, Geim AK, Morozov SV, Jiang D, Zhang Y, Dubonos SV, Grigorieva IV, Firsov AA. Electric field effect in atomically thin carbon films. *Science* 2004, 306:666–669.
2. Novoselov KS, Geim AK, Morozov SV, Jiang D, Katsnelson MI, Grigorieva IV, Dubonos SV, Firsov AA. Two-dimensional gas of massless Dirac Fermions in graphene. *Nature* 2005, 438:197–200.
3. Novoselov KS, McCann E, Morozov SV, Fal'ko VI, Katsnelson MI, Zeitler U, Jiang D, Schedin F, Geim AK. Unconventional quantum Hall effect and Berry's phase of 2 pi in bilayer graphene. *Nat Phys* 2006, 2:177–180.
4. Zhang YB, Tan YW, Stormer HL, Kim P. Experimental observation of the quantum Hall effect and Berry's phase in graphene. *Nature* 2005, 438:201–204.
5. Geim AK, Novoselov KS. The rise of graphene. *Nat Mater* 2007, 6:183–191.
6. Pang SP, Hernandez Y, Feng XL, Mullen K. Graphene as transparent electrode material for organic electronics. *Adv Mater* 2011, 23:2779–2795.
7. Gomez-Navarro C, Burghard M, Kern K. Elastic properties of chemically derived single graphene sheets. *Nano Lett* 2008, 8:2045–2049.
8. Calizo I, Balandin AA, Bao W, Miao F, Lau CN. Temperature dependence of the Raman spectra of graphene and graphene multilayers. *Nano Lett* 2007, 7:2645–2649.
9. Bae S, Kim H, Lee Y, Xu XF, Park JS, Zheng Y, Balakrishnan J, Lei T, Kim HR, Song YI, et al. Roll-to-roll production of 30-inch graphene films for transparent electrodes. *Nat Nanotechnol* 2010, 5:574–578.
10. Liu M, Yin XB, Ulin-Avila E, Geng BS, Zentgraf T, Ju L, Wang F, Zhang X. A graphene-based broadband optical modulator. *Nature* 2011, 474:64–67.
11. Robinson JT, Perkins FK, Snow ES, Wei ZQ, Sheehan PE. Reduced graphene oxide molecular sensors. *Nano Lett* 2008, 8:3137–3140.
12. Tang Q, Zhou Z, Chen ZF. Innovation and discovery of graphene-like materials via density-functional theory computations. *Wiley Interdiscip Rev Comput Mol Sci* 2015, 5:360–379.
13. Mak KF, Lee C, Hone J, Shan J, Heinz TF. Atomically thin MoS2: a new direct-gap semiconductor. *Phys Rev Lett* 2010, 105:136805.
14. Splendiani A, Sun L, Zhang YB, Li TS, Kim J, Chim CY, Galli G, Wang F. Emerging photoluminescence in monolayer MoS2. *Nano Lett* 2010, 10:1271–1275.
15. Banerjee S, Richardson W, Coleman J, Chatterjee A. *A New Three-Terminal Tunnel Device*, vol. 8. ETATS-UNIS: Institute of Electrical and Electronics Engineers: New York, NY; 1987, 347–349.
16. Li LK, Yu YJ, Ye GJ, Ge QQ, Ou XD, Wu H, Feng DL, Chen XH, Zhang YB. Black phosphorus field-effect transistors. *Nat Nanotechnol* 2014, 9:372–377.
17. Xia FN, Wang H, Jia YC. Rediscovering black phosphorus as an anisotropic layered material for optoelectronics and electronics. *Nat Commun* 2014, 5:4458.
18. Qiao JS, Kong XH, Hu ZX, Yang F, Ji W. High-mobility transport anisotropy and linear dichroism in few-layer black phosphorus. *Nat Commun* 2014, 5:4475.
19. Jing Y, Zhang X, Zhou Z. Phosphorene: what can we know from computations? *Wiley Interdiscip Rev Comput Mol Sci* 2016, 6:5–19.
20. Wang XB, Zhi CY, Li L, Zeng HB, Li C, Mitome M, Golberg D, Bando Y. "Chemical blowing" of thin-walled bubbles: high-throughput fabrication of large-area, few-layered BN and C-x-BN nanosheets. *Adv Mater* 2011, 23:4072–4076.
21. Ci L, Song L, Jin CH, Jariwala D, Wu DX, Li YJ, Srivastava A, Wang ZF, Storr K, Balicas L, et al. Atomic layers of hybridized boron nitride and graphene domains. *Nat Mater* 2010, 9:430–435.
22. Pakdel A, Wang XB, Zhi CY, Bando Y, Watanabe K, Sekiguchi T, Nakayama T, Golberg D. Facile synthesis of vertically aligned hexagonal boron nitride nanosheets hybridized with graphitic domains. *J Mater Chem* 2012, 22:4818–4824.
23. Wei XL, Wang MS, Bando Y, Golberg D. Electron-beam-induced substitutional carbon doping of boron

nitride nanosheets, nanoribbons, and nanotubes. *ACS Nano* 2011, 5:2916–2922.

24. Lin TW, Su CY, Zhang XQ, Zhang WJ, Lee YH, Chu CW, Lin HY, Chang MT, Chen FR, Li LJ. Converting graphene oxide monolayers into boron carbonitride nanosheets by substitutional doping. *Small* 2012, 8:1384–1391.
25. Gao YB, Zhang YF, Chen PC, Li YC, Liu MX, Gao T, Ma DL, Chen YB, Cheng ZH, Qju XH, et al. Toward single-layer uniform hexagonal boron nitride-graphene patchworks with zigzag linking edges. *Nano Lett* 2013, 13:3439–3443.
26. Coleman JN, Lotya M, O'Neill A, Bergin SD, King PJ, Khan U, Young K, Gaucher A, De S, Smith RJ, et al. Two-dimensional nanosheets produced by liquid exfoliation of layered materials. *Science* 2011, 331:568–571.
27. Feng J, Sun X, Wu CZ, Peng LL, Lin CW, Hu SL, Yang JL, Xie Y. Metallic few-layered VS2 ultrathin nanosheets: high two-dimensional conductivity for in-plane supercapacitors. *J Am Chem Soc* 2011, 133:17832–17838.
28. Feng J, Peng LL, Wu CZ, Sun X, Hu SL, Lin CW, Dai J, Yang JL, Xie Y. Giant moisture responsiveness of VS2 ultrathin nanosheets for novel touchless positioning interface. *Adv Mater* 2012, 24:1969–1974.
29. Sun YF, Cheng H, Gao S, Sun ZH, Liu QH, Liu Q, Lei FC, Yao T, He JF, Wei SQ, et al. Freestanding tin disulfide single-layers realizing efficient visible-light water splitting. *Angew Chem Int Ed Engl* 2012, 51:8727–8731.
30. Yu X, Li LL, Xu XW, Tang CC. Prediction of two-dimensional boron sheets by particle swarm optimization algorithm. *J Phys Chem C* 2012, 116:20075–20079.
31. Kirkpatrick S, Gelatt CD, Vecchi MP. Optimization by simulated annealing. *Science* 1983, 220:671–680.
32. Wille LT. Searching potential-energy surfaces by simulated annealing. *Nature* 1986, 324:46–47.
33. Doll K, Schon JC, Jansen M. Global exploration of the energy landscape of solids on the *ab initio* level. *Phys Chem Chem Phys* 2007, 9:6128–6133.
34. Deaven DM, Ho KM. Molecular-geometry optimization with a genetic algorithm. *Phys Rev Lett* 1995, 75:288–291.
35. Woodley SM, Battle PD, Gale JD, Catlow CRA. The prediction of inorganic crystal structures using a genetic algorithm and energy minimisation. *Phys Chem Chem Phys* 1999, 1:2535–2542.
36. Harris KDM, Johnston RL, Kariuki BM. The genetic algorithm: foundations and applications in structure solution from powder diffraction data. *Acta Crystallogr A* 1998, 54:632–645.
37. Woodley SM. Prediction of crystal structures using evolutionary algorithms and related techniques. In: Johnson RL, ed. *Applications of Evolutionary Computation in Chemistry*, vol. 110. Berlin: Springer-Verlag Berlin; 2004, 95–132.
38. Oganov AR, Glass CW. Evolutionary crystal structure prediction as a tool in materials design. *J Phys Condens Matter* 2008, 20:064210.
39. Lyakhov AO, Oganov AR, Stokes HT, Zhu Q. New developments in evolutionary structure prediction algorithm USPEX. *Comput Phys Commun* 2013, 184:1172–1182.
40. Ji M, Umemoto K, Wang CZ, Ho KM, Wentzcovitch RM. Ultrahigh-pressure phases of H2O ice predicted using an adaptive genetic algorithm. *Phys Rev B* 2011, 84:220105.
41. Wu SQ, Umemoto K, Ji M, Wang CZ, Ho KM, Wentzcovitch RM. Identification of post-pyrite phase transitions in SiO2 by a genetic algorithm. *Phys Rev B* 2011, 83:184102.
42. Wales DJ, Doye JPK. Global optimization by basin-hopping and the lowest energy structures of Lennard-Jones clusters containing up to 110 atoms. *J Phys Chem A* 1997, 101:5111–5116.
43. Goedecker S. Minima hopping: an efficient search method for the global minimum of the potential energy surface of complex molecular systems. *J Chem Phys* 2004, 120:9911–9917.
44. Martonak R, Laio A, Parrinello M. Predicting crystal structures: the Parrinello-Rahman method revisited. *Phys Rev Lett* 2003, 90:075503.
45. Martonak R, Laio A, Bernasconi M, Ceriani C, Raiteri P, Zipoli F, Parrinello M. Simulation of structural phase transitions by metadynamics. *Z Kristallogr* 2005, 220:489–498.
46. Pickard CJ, Needs RJ. High-pressure phases of silane. *Phys Rev Lett* 2006, 97:045504.
47. Pickard CJ, Needs RJ. Structure of phase III of solid hydrogen. *Nat Phys* 2007, 3:473–476.
48. Pickard CJ, Needs RJ. Highly compressed ammonia forms an ionic crystal. *Nat Mater* 2008, 7:775–779.
49. Wang YC, Lv JA, Zhu L, Ma YM. Crystal structure prediction via particle-swarm optimization. *Phys Rev B* 2010, 82:094116.
50. Wang YC, Lv J, Zhu L, Ma YM. CALYPSO: a method for crystal structure prediction. *Comput Phys Commun* 2012, 183:2063–2070.
51. Wang H, Wang YC, Lv J, Li Q, Zhang LJ, Ma YM. CALYPSO structure prediction method and its wide application. *Comput Mater Sci* 2016, 112:406–415.
52. Pickard CJ, Needs RJ. *Ab initio* random structure searching. *Phys Condens Matter* 2011, 23:053201.
53. Luo XY, Yang JH, Liu HY, Wu XJ, Wang YC, Ma YM, Wei SH, Gong XG, Xiang HJ. Predicting two-dimensional boron-carbon compounds by the global optimization method. *J Am Chem Soc* 2011, 133:16285–16290.

54. Luo W, Ma YM, Gong XG, Xiang HJ. Prediction of silicon-based layered structures for optoelectronic applications. *J Am Chem Soc* 2014, 136:15992–15997.
55. Zhou XF, Oganov AR, Wang ZH, Popov IA, Boldyrev AI, Wang HT. Two-dimensional magnetic boron. *Phys Rev B* 2016, 93:085406.
56. Zhao YC, Zeng SM, Ni J. Superconductivity in two-dimensional boron allotropes. *Phys Rev B* 2016, 93:014502.
57. Lebegue S, Bjorkman T, Klintenberg M, Nieminen RM, Eriksson O. Two-dimensional materials from data filtering and *ab initio* calculations. *Phys Rev X* 2013, 3:031002.
58. Stillinger FH. Exponential multiplicity of inherent structures. *Phys Rev E* 1999, 59:48–51.
59. Revard BC, Tipton WW, Hennig RG. Structure and stability prediction of compounds with evolutionary algorithms. In: AtahanEvrenk S, AspuruGuzik A, eds. *Prediction and Calculation of Crystal Structures: Methods and Applications*, vol. 345. Berlin: Springer-Verlag Berlin; 2014, 181–222.
60. Oganov AR, Lyakhov AO, Valle M. How evolutionary crystal structure prediction works-and why. *Acc Chem Res* 2011, 44:227–237.
61. d'Avezac M, Luo JW, Chanier T, Zunger A. Genetic-algorithm discovery of a direct-gap and optically allowed superstructure from indirect-gap Si and Ge semiconductors. *Phys Rev Lett* 2012, 108:027401.
62. Bahmann S, Kortus J. EVO-evolutionary algorithm for crystal structure prediction. *Comput Phys Commun* 2013, 184:1618–1625.
63. Lonie DC, Zurek E. XTALOPT: an open-source evolutionary algorithm for crystal structure prediction. *Comput Phys Commun* 2011, 182:372–387.
64. Glass CW, Oganov AR, Hansen N. USPEX—evolutionary crystal structure prediction. *Comput Phys Commun* 2006, 175:713–720.
65. Oganov AR, Glass CW. Crystal structure prediction using *ab initio* evolutionary techniques: principles and applications. *J Chem Phys* 2006, 124:244704.
66. Valle M, Oganov AR. *Crystal Structures Classifier for an Evolutionary Algorithm Structure Predictor*. IEEE Computer Society: Los Alamitos; 2008, 11–18.
67. Call ST, Zubarev DY, Boldyrev AI. Global minimum structure searches via particle swarm optimization. *J Comput Chem* 2007, 28:1177–1186.
68. Lv J, Wang YC, Zhu L, Ma YM. Particle-swarm structure prediction on clusters. *J Chem Phys* 2012, 137:084104.
69. Wang YC, Miao MS, Lv J, Zhu L, Yin KT, Liu HY, Ma YM. An effective structure prediction method for layered materials based on 2D particle swarm optimization algorithm. *J Chem Phys* 2012, 137:224108.
70. Lu SH, Wang YC, Liu HY, Miao MS, Ma YM. Self-assembled ultrathin nanotubes on diamond (100) surface. *Nat Commun* 2014, 5:3666.
71. Zhang XX, Wang YC, Lv J, Zhu CY, Li Q, Zhang M, Li Q, Ma YM. First-principles structural design of superhard materials. *J Chem Phys* 2013, 138:114101.
72. Zhang YY, Gao WG, Chen SY, Xiang HJ, Gong XG. Inverse design of materials by multi-objective differential evolution. *Comput Mater Sci* 2015, 98:51–55.
73. Storn R, Price K. Differential evolution—a simple and efficient heuristic for global optimization over continuous spaces. *J Glob Optim* 1997, 11:341–359.
74. Joshi R, Sanderson AC. Minimal representation multisensor fusion using differential evolution. *IEEE Trans Syst Man Cybern A Syst Hum* 1999, 29:63–76.
75. Luo W, Xiang HJ. Room temperature quantum spin hall insulators with a buckled square lattice. *Nano Lett* 2015, 15:3230–3235.
76. Trimarchi G, Zunger A. Global space-group optimization problem: finding the stablest crystal structure without constraints. *Phy Rev B* 2007, 75:104113.
77. Schon JC, Jansen M. First step towards planning of syntheses in solid-state chemistry: determination of promising structure candidates by global optimization. *Angew Chem Int Ed Engl* 1996, 35:1287–1304.
78. Giannozzi P, Baroni S, Bonini N, Calandra M, Car R, Cavazzoni C, Ceresoli D, Chiarotti GL, Cococcioni M, Dabo I, et al. QUANTUM ESPRESSO: a modular and open-source software project for quantum simulations of materials. *Phys Condens Matter* 2009, 21:395502.
79. Kresse G, Hafner J. *Ab initio* molecular-dynamics simulation of the liquid-metal amorphous-semiconductor transition in germanium. *Phy Rev B* 1994, 49:14251–14269.
80. Xiang HJ, Huang B, Kan EJ, Wei SH, Gong XG. Towards direct-gap silicon phases by the inverse band structure design approach. *Phys Rev Lett* 2013, 110:118702.
81. Tipton WW, Hennig RG. A grand canonical genetic algorithm for the prediction of multi-component phase diagrams and testing of empirical potentials. *Phys Condens Matter* 2013, 25:495401.
82. Revard BC, Tipton WW, Yesypenko A, Hennig RG. Grand-canonical evolutionary algorithm for the prediction of two-dimensional materials. *Phy Rev B* 2016, 93:054117.
83. Abraham NL, Probert MIJ. Improved real-space genetic algorithm for crystal structure and polymorph prediction. *Phy Rev B* 2008, 77:134117.
84. Kuhn HW. The Hungarian method for the assignment problem. *Naval Res Logistics* 2005, 52:7–21.

85. Johnston RL. Evolving better nanoparticles: genetic algorithms for optimising cluster geometries. *Dalton Trans* 2003, 22:4193–4207.
86. Oganov AR, Glass CW, Ono S. High-pressure phases of CaCO3: crystal structure prediction and experiment. *Earth Planet Sci Lett* 2006, 241:95–103.
87. Oganov AR, Valle M. How to quantify energy landscapes of solids. *J Chem Phys* 2009, 130:104504.
88. Baba N. Convergence of a random optimization method for constrained optimization problems. *J Optim Theory Appl* 1981, 33:451–461.
89. Dai J, Zhao Y, Wu XJ, Yang JL, Zeng XC. Exploration of structures of two-dimensional boron-silicon compounds with sp(2) silicon. *J Phys Chem Lett* 2013, 4:561–567.
90. Tan X, Li FY, Chen ZF. Metallic BSi3 silicene and its one-dimensional derivatives: unusual nanomaterials with planar aromatic D-6 h six-membered silicon rings. *J Phys Chem C* 2014, 118:25825–25835.
91. Hartke B. Global geometry optimization of clusters using genetic algorithms. *J Phys Chem* 1993, 97:9973–9976.
92. Wu XJ, Dai J, Zhao Y, Zhuo ZW, Yang JL, Zeng XC. Two-dimensional boron monolayer sheets. *ACS Nano* 2012, 6:7443–7453.
93. Lu HG, Mu YW, Bai H, Chen Q, Li SD. Binary nature of monolayer boron sheets from *ab initio* global searches. *J Chem Phys* 2013, 138:024701.
94. Wang ZH, Zhou XF, Zhang XM, Zhu Q, Dong HF, Zhao MW, Oganov AR. Phagraphene: a low-energy graphene allotrope composed of 5-6-7 carbon rings with distorted Dirac cones. *Nano Lett* 2015, 15:6182–6186.
95. Xiang HJ, Wei SH, Gong XG. Structural motifs in oxidized graphene: a genetic algorithm study based on density functional theory. *Phys Rev B* 2010, 82:035416.
96. Xiang HJ, Huang B, Li ZY, Wei SH, Yang JL, Gong XG. Ordered semiconducting nitrogen-graphene alloys. *Phys Rev X* 2012, 2:011003.
97. Li PF, Zhou RL, Zeng XC. The search for the most stable structures of silicon-carbon monolayer compounds. *Nanoscale* 2014, 6:11685–11691.
98. Yang LM, Bacic V, Popov IA, Boldyrev AI, Heine T, Frauenheim T, Ganz E. Two-dimensional Cu2Si monolayer with planar hexacoordinate copper and silicon bonding. *J Am Chem Soc* 2015, 137:2757–2762.
99. Zhou LJ, Zhang YF, Wu LM. SiC2 siligraphene and nanotubes: novel donor materials in excitonic solar cells. *Nano Lett* 2013, 13:5431–5436.
100. Dai J, Wu XJ, Yang JL, Zeng XC. AlxC monolayer sheets: two-dimensional networks with planar tetracoordinate carbon and potential applications as donor materials in solar cell. *J Phys Chem Lett* 2014, 5:2058–2065.
101. Ding Y, Wang YL. Geometric and electronic structures of two-dimensional SiC3 compound. *J Phys Chem C* 2014, 118:4509–4515.
102. Li YF, Liao YL, Schleyer PV, Chen ZF. Al2C monolayer: the planar tetracoordinate carbon global minimum. *Nanoscale* 2014, 6:10784–10791.
103. Zhang M, Gao GY, Kutana A, Wang YC, Zou XL, Tse JS, Yakobson BI, Li HD, Liu HY, Ma YM. Two-dimensional boron-nitrogen-carbon monolayers with tunable direct band gaps. *Nanoscale* 2015, 7:12023–12029.
104. Li YF, Liao YL, Chen ZF. Be2C monolayer with quasi-planar hexacoordinate carbons: a global minimum structure. *Angew Chem Int Ed Engl* 2014, 53:7248–7252.
105. Wang Y, Li F, Li YF, Chen ZF. Semi-metallic Be5C2 monolayer global minimum with quasi-planar pentacoordinate carbons and negative Poisson's ratio. *Nat Commun* 2016, 7:11488.
106. Zhang H, Li Y, Hou J, Du A, Chen Z. Dirac state in the FeB2 monolayer with graphene-like boron sheet. *Nano Lett* 2016, 16:6124–6129.
107. Zhang HJ, Li YF, Hou JH, Tu KX, Chen ZF. FeB6 monolayers: the graphene-like material with hypercoordinate transition metal. *J Am Chem Soc* 2016, 138:5644–5651.
108. Way BM, Dahn JR, Tiedje T, Myrtle K, Kasrai M. Preparation and characterization of BXC1-X thin-films with the graphite structure. *Phys Rev B* 1992, 46:1697–1702.
109. Hu QK, Wu QH, Ma YM, Zhang LJ, Liu ZY, He JL, Sun H, Wang HT, Tian YJ. First-principles studies of structural and electronic properties of hexagonal BC5. *Phys Rev B* 2006, 73:214116.
110. Wu XJ, Pei Y, Zeng XC. B2C graphene, nanotubes, and nanoribbons. *Nano Lett* 2009, 9:1577–1582.
111. Zhao LY, He R, Rim KT, Schiros T, Kim KS, Zhou H, Gutierrez C, Chockalingam SP, Arguello CJ, Palova L, et al. Visualizing individual nitrogen dopants in monolayer graphene. *Science* 2011, 333:999–1003.
112. Zhou XF, Dong X, Oganov AR, Zhu Q, Tian YJ, Wang HT. Semimetallic two-dimensional boron allotrope with massless Dirac Fermions. *Phys Rev Lett* 2014, 112:085502.
113. Guo ZX, Zhang YY, Xiang HJ, Gong XG, Oshiyama A. Structural evolution and optoelectronic applications of multilayer silicene. *Phys Rev B* 2015, 92:201413.
114. Yang JH, Zhang YY, Yin WJ, Gong XG, Yakobson BI, Wei SH. Two-dimensional SiS layers with promising electronic and optoelectronic properties: theoretical prediction. *Nano Lett* 2016, 16:1110–1117.

115. Zhou DW, Pu CY, He CZ, Zhang FW, Lu C, Bao G. Pressure-induced phase transition of BiOF: novel two-dimensional layered structures. *Phys Chem Chem Phys* 2015, 17:4434–4440.

116. Gao B, Shao XC, Lv J, Wang YC, Ma YM. Structure prediction of atoms adsorbed on two-dimensional layer materials: method and applications. *J Phys Chem C* 2015, 119:20111–20118.

117. Ma FX, Gao GP, Jiao YL, Gu YT, Bilic A, Zhang HJ, Chen ZF, Du AJ. Predicting a new phase (T ") of two-dimensional transition metal dichalcogenides and strain-controlled topological phase transition. *Nanoscale* 2016, 8:4969–4975.

118. Luo W, Xiang H. Two-Dimensional Phosphorus Oxides as Energy and Information Materials. *Angew Chem Int Ed Engl* 2016, 55:8575–8580.

119. Wang Y, Li YF, Chen ZF. Not your familiar two dimensional transition metal disulfide: structural and electronic properties of the PdS2 monolayer. *J Mater Chem C* 2015, 3:9603–9608.

120. Huang B, Deng HX, Lee H, Yoon M, Sumpter BG, Liu F, Smith SC, Wei SH. Exceptional optoelectronic properties of hydrogenated bilayer silicene. *Phys Rev X* 2014, 4:021029.

121. Tritsaris GA, Kaxiras E, Meng S, Wang EG. Adsorption and diffusion of lithium on layered silicon for Li-ion storage. *Nano Lett* 2013, 13:2258–2263.

122. Sakai Y, Oshiyama A. Structural stability and energy-gap modulation through atomic protrusion in free-standing bilayer silicene. *Phys Rev B* 2015, 91:201405.

123. Ziletti A, Carvalho A, Campbell DK, Coker DF, Neto AHC. Oxygen defects in phosphorene. *Phys Rev Lett* 2015, 114:046801.

124. Ziletti A, Carvalho A, Trevisanutto PE, Campbell DK, Coker DF, Neto AHC. Phosphorene oxides: bandgap engineering of phosphorene by oxidation. *Phy Rev B* 2015, 91:085407.

125. Lu JP, Wu J, Carvalho A, Ziletti A, Liu HW, Tan JY, Chen YF, Neto AHC, Ozyilmaz B, Sow CH. Bandgap engineering of phosphorene by laser oxidation toward functional 2D materials. *ACS Nano* 2015, 9:10411–10421.

126. Wang GX, Pandey R, Karna SP. Phosphorene oxide: stability and electronic properties of a novel two-dimensional material. *Nanoscale* 2015, 7:524–531.

127. Garrity KF, Rabe KM, Vanderbilt D. Hyperferroelectrics: proper ferroelectrics with persistent polarization. *Phys Rev Lett* 2014, 112:127601.

128. Qian XF, Liu JW, Fu L, Li J. Quantum spin Hall effect in two-dimensional transition metal dichalcogenides. *Science* 2014, 346:1344–1347.

129. Bernevig BA, Hughes TL, Zhang SC. Quantum spin Hall effect and topological phase transition in HgTe quantum wells. *Science* 2006, 314:1757–1761.

130. Hybertsen MS, Louie SG. 1st-principles theory of quasi-particles—calculation of band-gaps in semiconductors and insulators. *Phys Rev Lett* 1985, 55:1418–1421.

131. Mattson EC, Pu HH, Cui SM, Schofield MA, Rhim S, Lu GH, Nasse MJ, Ruoff RS, Weinert M, Gajdardziska-Josifovska M, et al. Evidence of nanocrystalline semiconducting graphene monoxide during thermal reduction of graphene oxide in vacuum. *ACS Nano* 2011, 5:9710–9717.

132. Zhang QY, Cheng LJ. Structural determination of (Al2O3)(n) (n = 1-15) clusters based on graphic processing unit. *J Chem Inf Model* 2015, 55:1012–1020.

